International Journal of Fracture **50:** 239–262, 1991.
© 1991 *Kluwer Academic Publishers. Printed in the Netherlands.*

Green's functions for dislocations in bonded strips and related crack problems

R. BALLARINI and H.A. LUO
Department of Civil Engineering, Case Western Reserve University, Cleveland, Ohio 44106, USA

Received 30 April 1990; accepted 30 September 1990

Abstract. Green's functions are derived for the plane elastostatics problem of a dislocation in a bimaterial strip. Using these fundamental solutions as kernels, various problems involving cracks in a bimaterial strip are analyzed using singular integral equations. For each problem considered, stress intensity factors are calculated for several combinations of the parameters which describe loading, geometry and material mismatch.

1. Introduction

The mechanical behavior of bimaterial interfaces in composite materials is currently a topic of considerable interest to the applied mechanics community. Many analytical, numerical and experimental investigations have been conducted recently to gain a better understanding of how these interfaces affect bulk composite properties such as strength, stiffness and toughness. The mechanisms of cracking or debonding along bimaterial interfaces are of particular interest in brittle composites since it has been established experimentally and through micromechanical models that certain desired properties can only be achieved in such materials if the cracks which initiate in the matrix are deflected by the fibers along the fiber-matrix interface [1]. It is clear that micromechanical analyses will continue to play an important role in analyzing and designing brittle composites to ensure this desired failure sequence. Moreover, experimental programs are necessary to measure the fracture toughness of the fiber-matrix interface because the conditions required for the desired behavior involve the relative toughness between the fiber and the interface.

Micromechanical models which involve relatively simple geometries such as cracks in infinite and semi-infinite plane bodies have been handled using distributed dislocations and singular integral equations [2]. For complicated finite geometries, on the other hand, the finite element method has gained popularity [3, 4]. The singular integral equation method has two advantages. First, it leads to accurate results for stress intensity factors. Second, once the Green's functions are derived and the equations are set up, parameter studies can be performed by simply varying the dimensionless parameters which describe the loading, crack length and geometry. Unfortunately, if the geometry of the problem is complicated, the method is not feasible because it is very difficult to derive the kernels. The real advantage of the finite element method is its ability to model complicated geometries. If proper care is taken, the method also produces accurate results. Parameter studies, on the other hand, are time consuming and relatively cumbersome.

This paper addresses a class of problems which involve cracks in bonded strips. The motivation of this work came from a desire to develop a computer program which could be used to calculate stress intensity factors and energy release rates for bimaterial fracture specimens being developed at C.W.R.U., and model the geometry of the so-called Santa Barbara mixed-mode specimen shown in Fig. 1a. The latter 'T-crack' configuration was

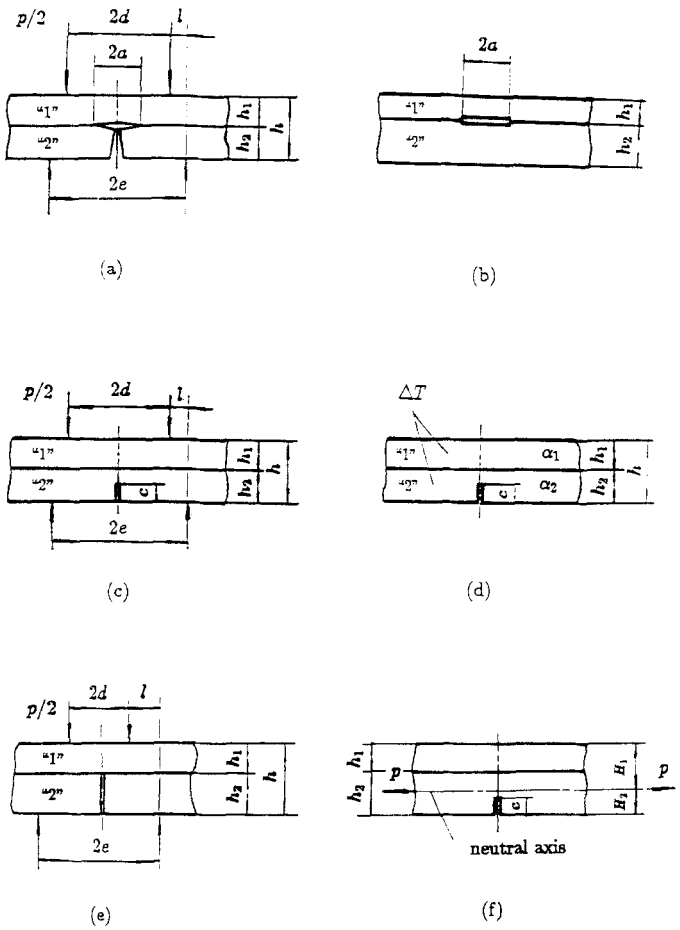

Fig. 1. Crack configurations for the bimaterial strip.

developed by Charalambides et al. [3, 4] at the University of California at Santa Barbara to measure the fracture resistance of bimaterial interfaces. To interpret experimental results and to guide the design of the specimen, they developed a finite element approach to characterize trends in stress intensity factors, energy release rates and center point displacements with specimen dimensions, elastic properties and crack length. As discussed in [3, 4], the stress intensity factors and energy release rate for the crack growing along the interface exhibit steady state behavior as a result of the constant moment within the inner loading points. The shortest crack for which results were calculated in [3, 4] is approximately $a/l = 0.0938$ (or $a/h_2 = 0.3127$). The results showed that this crack length is already at steady state. One of the questions left unanswered is: how long does the crack have to grow along the interface before it reaches steady state? To answer this question the problem is modeled in this paper using the singular integral equation technique. Results will be presented for relatively short crack lengths as well as for the case $a = 0$, $c \leqslant h_2$ (Fig. 1c–e). It should be noted that at the end of this work the authors learned that Charalambides has recently obtained results for both the transient region and for the three-point loading configuration.

In the next section Green's functions are derived for edge dislocations in a bimaterial strip. These fundamental solutions can be used in turn to set up the integral equations for all the configurations shown in Fig. 1. It should be noted that this class of problems has been analyzed by Lu [5] and Lu and Erdogan [6] using Fourier transforms. In [5, 6] the problems were reduced to singular integral equations without the use of dislocations as fundamental solutions. Dislocation densities, however, were defined eventually to set up the integral equations. In this paper the dislocations are introduced as fundamental solutions. This will enable us, in the future, to solve problems which involve non-symmetric loading and/or inclined cracks. In the third section the dislocation solutions are used to set up the integral equations for several configurations and loadings. The last section presents numerical results and comparisons with existing solutions.

2. Fundamental solutions and loading conditions

Assume that two dissimilar elastic strips are bonded along the x axis. The upper layer ($y > 0$) is labeled by '1' and the lower layer ($y < 0$) is labeled by '2'. The Green's functions for an edge dislocation in the bimaterial strip are derived by superposing the solutions for (1) a dislocation near the interface of two bonded half-planes; and (2) a bimaterial strip loaded with boundary tractions which cancel out those induced by problem (1).

The solution to problem (1) is well known. The stresses and displacements, which will be denoted by superscript '(1)', can be expressed conveniently in terms of Muskhelishvili's complex potentials as

$$\begin{aligned}
(\sigma_{yy}^{(1)} - i\sigma_{xy}^{(1)})_i &= \Phi_i + \overline{\Phi_i(z)} + z\overline{\Phi_i'(z)} + \overline{\Psi_i(z)},\\
(\sigma_{yy}^{(1)} + \sigma_{xx}^{(1)})_i &= 2[\Phi_i(z) + \overline{\Phi_i(z)}],\\
2\mu_i\left(\frac{\partial u^{(1)}}{\partial x} + i\frac{\partial v^{(1)}}{\partial x}\right)_i &= \kappa_i\Phi_i(z) - [\overline{\Phi_i(z)} + z\overline{\Phi_i'(z)} + \overline{\Psi_i(z)}],
\end{aligned} \tag{1}$$

in which the subscript i ($i = 1, 2$) denotes 'in region i'; Φ_1 and Ψ_1 correspond to the potentials for the upper half plane and Φ_2 and Ψ_2 correspond to the potentials for the lower half plane. Moreover, z is the complex variable $x + iy$, the prime denotes differentiation with respect to z, an overbar denotes conjugation, μ is the shear modulus, and κ is defined in terms of Poisson's ratio ν as $\kappa = 3 - 4\nu$ for plane strain, and $\kappa = (3 - \nu)/(1 + \nu)$ for plane stress. The complex-potentials for a dislocation located at $z_0 = x_0 + iy_0$ are given by [7]

$$\Phi_i = \Phi_i^D + \Phi_i^C, \quad \Psi_i = \Psi_i^D + \Psi_i^C, \tag{2}$$

with

$$\Phi_1^D = \Psi_1^D = 0, \quad \Phi_1^C = \frac{(1+\alpha)}{(1-\beta)}\frac{A}{(z - z_0)},$$

$$\Psi_1^C = -\Phi_1^C - z\Phi_1^{C'} + \frac{1+\alpha}{1+\beta}\left[\frac{\bar{A}}{z - z_0} + A\frac{\bar{z}_0 - z_0}{(z - z_0)^2}\right],$$

$$\Phi_2^D = \frac{A}{z - z_0}, \quad \Psi_2^D = A\frac{\overline{z_0}}{(z - z_0)^2} + \frac{\bar{A}}{z - z_0},$$

$$\Phi_2^C = \frac{\alpha - \beta}{1 + \beta}\left[\frac{A}{z - \bar{z}_0} + \bar{A}\frac{(z - \bar{z}_0)}{(z - \bar{z}_0)^2}\right],$$

$$\Psi_2^C = -\Phi_2^C - z\Phi_2^{C'} + \frac{\alpha + \beta}{1 - \beta}\frac{\bar{A}}{z - \bar{z}_0} + \frac{\bar{A}}{z - z_0} + A\frac{(\bar{z}_0 - z_0)}{(z - z_0)^2}. \tag{3}$$

In (3) the Dundurs constants α and β are defined by

$$\alpha = \frac{\mu_1(\kappa_2 + 1) - \mu_2(\kappa_1 + 1)}{\mu_1(\kappa_2 + 1) + \mu_2(\kappa_1 + 1)},$$

$$\beta = \frac{\mu_1(\kappa_2 - 1) - \mu_2(\kappa_1 - 1)}{\mu_1(\kappa_2 + 1) + \mu_2(\kappa_1 + 1)}, \tag{4}$$

and

$$A = \frac{C}{2\pi i}\frac{(1 - \beta^2)}{(1 - \alpha)}b, \quad C = \frac{2\mu_1(1 - \alpha)}{(\kappa_1 + 1)(1 - \beta^2)}, \tag{5}$$

where $b = b_x + ib_y$ with b_x and b_y being the x and y components of the Burgers vector. We next compute the stresses due to a dislocation $b_1 = b_{1x} + ib_{1y}$ at the interface ($z_0 \to 0$) and due to a dislocation $b_2 = b_{2x}$ located at $x = 0$, $y = \zeta < 0$. The first dislocation corresponds to the Green's function for the interface crack, while the second corresponds to the fundamental solution for the vertical crack. For $z_0 \to 0$, the stresses become

$$\sigma_{xy}^{(1)} + i\sigma_{yy}^{(1)} = \left[\frac{C}{\pi}\frac{1}{x} - i\beta C\delta(x)\right]b_1 \tag{6}$$

for $y = 0$,

$$\sigma_{xy}^{(1)} + i\sigma_{yy}^{(1)} = \frac{C}{\pi}\left(\frac{x}{r^2} - i\beta\frac{y}{r^2}\right)b_1 - \frac{C}{\pi}(1 + \beta)\left[\frac{2xy^2}{r^4} + i\left(\frac{2y^3}{r^4} - \frac{y}{r^2}\right)\right]\bar{b}_1 \tag{7}$$

for $y > 0$, and

$$\sigma_{xy}^{(1)} + i\sigma_{yy}^{(1)} = \frac{C}{\pi}\left(\frac{x}{r^2} + i\beta\frac{y}{r^2}\right)b_1 - \frac{C}{\pi}\left(1 - \beta\right)\left[\frac{2xy^2}{r^4} + i\left(\frac{2y^3}{r^4} - \frac{y}{r^2}\right)\right]\bar{b}_1,$$

$$\sigma_{xx}^{(1)} = \frac{C}{\pi}\Re[D(y, x)b_1], \tag{8}$$

with

$$D(y, x) = (1 - \beta)\frac{2y^3}{r^4} - (3 - 2\beta)\frac{y}{r^2} - i\left[(1 - 2\beta)\frac{x}{r^2} - (1 - \beta)\frac{2xy^2}{r^4}\right] \tag{9}$$

for $y < 0$, where $\delta(x)$ is the Dirac delta function. Here, some care must be taken during performing the limit [8]. Meanwhile, for dislocation b_2, it can be shown that

$$\sigma_{xy}^{(1)} + i\sigma_{yy}^{(1)} = -\frac{C}{\pi}\left[\frac{2x(y-\zeta)^2}{r_1^4} - \frac{x}{r_1^2} + \beta\frac{2x(y-\zeta)^2}{r_1^4} + 4\beta\zeta\frac{x(y-\zeta)}{r_1^4}\right]b_2$$
$$-i\frac{C}{\pi}\left[\frac{2(y-\zeta)^3}{r_1^4} - \frac{y-\zeta}{r_1^2} + 2\beta\frac{(y-\zeta)^3}{r_1^4} + 4\beta\zeta\frac{(y-\zeta)^2}{r_1^4} - 2\beta\zeta\frac{1}{r_1^2}\right]b_2 \tag{10}$$

for $y \geqslant 0$,

$$\sigma_{xy}^{(1)} + i\sigma_{yy}^{(1)} = -\frac{C}{\pi(1+\alpha)}\left\{(1-\beta^2)\left(\frac{2(y-\zeta)^2x}{r_1^4} - \frac{x}{r_1^2}\right) + (\alpha+\beta^2)\left(\frac{2(\zeta+y)^2x}{r_2^4} - \frac{x}{r_2^2}\right)\right.$$
$$-(1+\alpha)\beta\frac{2(\zeta+y)^2x}{r_2^4} + (\alpha-\beta)(1-\beta)\zeta\left(\frac{4(\zeta+y)x}{r_2^4} - \frac{16(\zeta+y)^3x}{r_2^6}\right)$$
$$\left.+2(\alpha-\beta)(1-\beta)\zeta^2\left(\frac{8(\zeta+y)^2x}{r_2^6} - \frac{2x}{r_2^4}\right)\right\}b_2,$$
$$+i\frac{C}{\pi(1+\alpha)}\left[(1-\beta^2)\left(\frac{y-\zeta}{r_1^2} - \frac{2(y-\zeta)^3}{r_1^4}\right) - (\alpha+\beta^2)\right.$$
$$\times\left(\frac{2(\zeta+y)^3}{r_2^4} - \frac{\zeta+y}{r_2^2}\right) + (1+\alpha)\beta\frac{2(\zeta+y)^3}{r_2^4} - 2(\alpha-\beta)(1-\beta)\zeta\frac{1}{r_2^2}$$
$$-(\alpha-\beta)(1-\beta)\zeta\left(\frac{8(\zeta+y)^2}{r_2^4} - \frac{16(\zeta+y)^4}{r_2^6}\right)$$
$$\left.+2(\alpha-\beta)(1-\beta)\zeta^2\left(\frac{6(\zeta+y)}{r_2^4} - \frac{8(\zeta+y)^3}{r_2^6}\right)\right]b_2 \tag{11}$$

for $y \leqslant 0$, where

$$r_1^2 = x^2 + (y-\zeta)^2, \quad r_2^2 = x^2 + (y+\zeta)^2. \tag{12}$$

In particular, when $y = 0$

$$\sigma_{xy}^{(1)}(x,0) + i\sigma_{yy}^{(1)}(x,0) = \frac{C}{\pi}E(x,\zeta)b_2, \tag{13}$$

with

$$E(x,\zeta) = \frac{x+i\zeta}{r_*^2} - 2(1-\beta)x\zeta\frac{\zeta+ix}{r_*^4}, \tag{14}$$

where $r_*^2 = x^2 + \zeta^2$; and when $y < 0$

$$\sigma_{xx}^{(1)}(0, y) = -\frac{C(1-\beta^2)}{\pi(1+\alpha)}\left[\frac{1}{y-\zeta} + F(y, \zeta)\right]b_2, \tag{15}$$

where

$$F(y, \zeta) = \frac{(\alpha+\beta^2)}{(1-\beta^2)}\frac{1}{y+\zeta} + \frac{2(\alpha-\beta)}{1+\beta}\frac{\zeta}{(y+\zeta)^2} - \frac{4(\alpha-\beta)}{1+\beta}\frac{\zeta^2}{(y+\zeta)^3}. \tag{16}$$

The solution to problem (2) is obtained by using Fourier transformation techniques. Without loss of generality, consider a bimaterial strip loaded with surface tractions which are symmetric about the y-axis. The Fourier transform of displacement is as follows:

$$U_i(\xi, y) = \int_0^\infty u_i(x, y) \sin \xi x \, dx,$$
$$V_i(\xi, y) = \int_0^\infty v_i(x, y) \cos \xi x \, dx. \tag{17}$$

The general solutions for U_i and V_i are [9]:

$$U_i(\xi, y) = (A_{i1}h_2 + A_{i2}y)e^{-\xi y} + (A_{i3}h_2 + A_i y)e^{\xi y},$$
$$V_i(\xi, y) = [A_{i1}h_2 + (\kappa_i/\xi + y)A_{i2}]e^{-\xi y} + [-A_{i3}h_2 + (\kappa_i/\xi - y)A_{i4}]e^{\xi y}, \tag{18}$$

with the unknown coefficients determined by continuity and boundary conditions along the interface:

$$A_{11} + A_{13} - A_{21} - A_{23} = 0,$$

$$A_{11} + \frac{\kappa_1}{\xi h_2}A_{12} - A_{13} + \frac{\kappa_1}{\xi h_2}A_{14} - A_{21} - \frac{\kappa_2}{\xi h_2}A_{22} + A_{23} - \frac{\kappa_2}{\xi h_2}A_{24} = 0,$$

$$\xi h_2 A_{11} + 2(1-\nu_1)A_{12} + \xi h_2 A_{13} - 2(1-\nu_1)A_{14} - \frac{\mu_2}{\mu_1} \times [\xi h_2 A_{21} + 2(1-\nu_2)A_{22} + \xi h_2 A_{23} - 2(1-\nu_2)A_{24}] = 0,$$

$$\xi h_2 A_{11} + (1-2\nu_1)A_{12} - \xi h_2 A_{13} + (1-2\nu_1)A_{14} - \frac{\mu_2}{\mu_1} \times [\xi h_2 A_{21} + (1-2\nu_2)A_{22} - \xi h_2 A_{23} + (1-2\nu_2)A_{24}] = 0,$$

$$-[\xi(A_{11}h_2 + A_{12}h_1) + 2(1-\nu_1)A_{12}]e^{-\xi h_1} + [-\xi(A_{13}h_2 + A_{14}h_1) + 2(1-\nu_1)A_{14}]e^{\xi h_1} = f_1(\xi),$$

$$-[\xi(A_{11}h_2 + A_{12}h_1) + (1-2\nu_1)A_{12}]e^{-\xi h_1} + [\xi(A_{13}h_2 + A_{14}h_1) - (1-2\nu_1)A_{14}]e^{\xi h_1} = f_2(\xi),$$

$$-[\xi h_2(A_{21}-A_{22})+2(1-\nu_2)A_{22}]e^{\xi h_2}+[-\xi h_2(A_{23}-A_{24})$$
$$+2(1-\nu_2)A_{24}]e^{-\xi h_2}=f_3(\xi),$$
$$-[\xi h_2(A_{21}-A_{22})+(1-2\nu_2)A_{22}]e^{\xi h_2}+[\xi h_2(A_{23}-A_{24})$$
$$-(1-2\nu_2)A_{24}]e^{-\xi h_2}=f_4(\xi), \tag{19}$$

where the first four equations represent the continuity of u, v, σ_{yy} and σ_{xy} along the interface, respectively; the last four equations specify the boundary conditions at $y=h_1$ and $y=-h_2$. The functions $f_1(\xi)$ and $f_2(\xi)$ are related to the Fourier transforms of the loadings on the top surface of the upper strip, while $f_3(\xi)$ and $f_4(\xi)$ are related to the Fourier transforms of the loadings on the bottom surface of the lower strip. To eliminate the unwanted surface traction along the boundaries due to each dislocation, for example b_x, in problem (1), functions $f_1(\xi)$, $f_2(\xi)$, $f_3(\xi)$ and $f_4(\xi)$ are set to be

$$f_1(\xi)=-\frac{1}{2\mu_1}\int_0^\infty \sigma_{yy}^{(1)}(x,h_1)\cos\xi x\,dx,$$
$$f_2(\xi)=-\frac{1}{2\mu_1}\int_0^\infty \sigma_{xy}^{(1)}(x,h_1)\sin\xi x\,dx,$$
$$f_3(\xi)=-\frac{1}{2\mu_2}\int_0^\infty \sigma_{yy}^{(1)}(x,-h_2)\cos\xi x\,dx,$$
$$f_4(\xi)=-\frac{1}{2\mu_2}\int_0^\infty \sigma_{xy}^{(1)}(x,-h_2)\sin\xi x\,dx. \tag{20}$$

It can be shown that Eqns. (19) are also applicable to the anti-symmetric problem. The $f_i(\xi)$'s have been evaluated for each case and are given in the Appendix.

After the A_{ij}'s are solved, the stress components due to problem (2), which are denoted by superscripts '(2)', are readily obtained by inverse Fourier transformation. For the symmetric problem, e.g. for dislocation b_x,

$$\sigma_{xy}^{(2)}(x,0)=\frac{4\mu_1 b_x}{\pi}\int_0^\infty [\xi h_2(A_{13}-A_{11})-(1-2\nu_1)(A_{12}+A_{14})]\times\sin\xi x\,d\xi,$$
$$\sigma_{yy}^{(2)}(x,0)=\frac{4\mu_1 b_x}{\pi}\int_0^\infty [-\xi h_2(A_{11}+A_{13})+2(1-\nu_1)(A_{14}-A_{12})]\times\cos\xi x\,d\xi \tag{21}$$

and

$$\sigma_{xx}^{(2)}(x,\ y)=\frac{4\mu_2 b_x}{\pi}\int_0^\infty \{[\xi(A_{21}h_2+A_{22}y)-2\nu_2 A_{22}]e^{-\xi y}+[\xi(A_{23}h_2+A_{24}y)$$
$$+2\nu_2 A_{24}]e^{\xi y}\}\cos\xi x\,d\xi \tag{22}$$

where $y<0$. For the anti-symmetric problem, e.g. for dislocation b_y, the above relationship is still valid if $\sin\xi x$ is replaced by $\cos\xi x$ and $\cos\xi x$ is replaced by $-\sin\xi x$.

For convenience, in subsequent discussions introduce the following definitions for the stresses produced by problem (2):

$$\sigma_{xy}^{(2)}(x,0) + i\sigma_{yy}^{(2)}(x,0) \equiv G_1(x)b_{1x} + G_2(x)b_{1y} + G_3(x;\zeta)b_{2x}$$
$$\sigma_{xx}^{(2)}(x,\ y) \equiv H_1(y;x)b_{1x} + H_2(y;x)b_{1y} + H_3(y;\zeta,x)b_{2x}. \tag{23}$$

We wish to point out that the fundamental solutions derived above can be used to solve a large class of problems. The purpose of this paper is to present the methodology. Thus we will consider only three types of loadings. These include three and four point bending (Fig. 1a), constant pressure along the crack surfaces, and a temperature change of the composite strip (Fig. 1d). Consider first a perfectly bonded bimaterial beam subjected to four-point bending. The stresses in the strip due to this loading condition can be calculated using composite beam theory if the strip is long enough. However, since we may be interested, in the future, in analyzing relatively short beams, an elasticity solution is obtained in the same manner as for problem (2) of the dislocation solution. The applied loads are represented by Dirac delta functions at the load points. That is $\sigma_{yy}(x,h_1) = -p[\delta(x-d)+\delta(x+d)]/2$ and $\sigma_{yy}(x,-h_2) = -p[\delta(x-e)+\delta(x+e)]/2$. The functions f_1, f_2, f_3, and f_4 for this case are listed in the Appendix. To evaluate the stresses which arise from this loading, it may seem natural to proceed in the same exact manner as for the dislocation solutions. However, tremendous care must be taken when evaluating the stresses along the interface and along the line $x = 0$ due to this loading condition, because the integrals in the inverse transformations converge very slowly. To improve the convergence the integrands are first evaluated at $\xi = \infty$. The dominant portion of these limits, which correspond to half-space solutions, are subtracted from and added to the integrands, and the added integrals are evaluated in closed form. The same procedure is also applied to the dislocation b_2 when it is close to the bottom surface. For brevity the details of the procedure are not given here, but can be recovered in similar analyses presented in [10, 11].

Denote the stresses produced by the four point bending as

$$\sigma_{xy}(x,0) + i\sigma_{yy}(x,0) \equiv pQ(x)/h_2,$$
$$\sigma_{xx}(0,\ y) \equiv pR(y)/h_2 \tag{24}$$

respectively, where p is the force per unit thickness. These will be used in Section 3 to set up the integral equations.

The next loading condition consists of a uniform change of temperature ΔT of the composite strip. The thermal stresses in the strip are calculated using beam theory [12]. In particular, the stress in layer 2 along the line $x = 0$ is given in terms of the thermal expansion coefficients α_1 and α_2 by

$$\sigma_{xx} = -(\alpha_2 - \alpha_1)\Delta T E_2^*\left(1 + \frac{3}{2}\frac{y}{h_2}\right)\Big/\left(1 + \frac{E_2^* h_2}{E_1^* h_1}\right), \tag{25}$$

with

$$E^* = \frac{E}{1-\nu^2}.$$

3. Integral equations

Several problem configurations are depicted in Fig. 1. The coordinate system is chosen such that the x-axis lies along the interface of the bimaterial strip, and the y-axis along the vertical crack so that layer 1 is at $y > 0$ and layer 2 is at $y < 0$. The integral equations for the four point bending problem shown in Fig. 1a are set up first. The stresses along the lines $y = 0$ and $x = 0$ ($y \leqslant 0$) are given by the summation of contributions from problem (1), problem (2) and the four point bend load (24). Replacing the dislocations by a distribution of dislocations enables us to satisfy the traction boundary conditions along the crack. This procedure leads to the following set of coupled singular integral equations:

$$\int_{-1}^{1} \frac{B_1(t_0)}{t - t_0}\,\mathrm{d}t_0 - i\beta\pi B_1(t) + \int_{-1}^{1} K_1(t, t_0)B_1(t_0)\,\mathrm{d}t_0$$
$$+ \int_{-1}^{1} K_2(t, t_0)\bar{B}_1(t_0)\,\mathrm{d}t_0 + \int_{-1}^{1} K_3(t, t_0)B_2(t_0)\,\mathrm{d}t_0 = p_1(t),$$
$$\int_{-1}^{1} \frac{B_2(t_0)}{t - t_0}\,\mathrm{d}t_0 + \int_{-1}^{1} K_4(t, t_0)B_2(t_0)\,\mathrm{d}t_0 + \int_{-1}^{1} K_5(t, t_0)B_1(t_0)\,\mathrm{d}t_0$$
$$+ \int_{-1}^{1} K_6(t, t_0)\bar{B}_1(t_0)\,\mathrm{d}t_0 = p_2(t), \tag{26}$$

together with the conjugate of the first equation in (26) where the dislocation densities are given by $B_1(t) = B_{1x}(at) + iB_{1y}(at)$ and $B_2(t) = B_{2x}(h_2(t-1)/2)$ with

$$B_{1x}(x) = -\frac{Ch_2}{P}\frac{\partial}{\partial x}[u(x, 0^+) - u(x, 0^-)],$$
$$B_{1y}(x) = -\frac{Ch_2}{P}\frac{\partial}{\partial x}[v(x, 0^+) - v(x, 0^-)],$$
$$B_{2x}(y) = -\frac{Ch_2}{p}\frac{\partial}{\partial y}[u(0^+, y) - u(0^-, y)]. \tag{27}$$

and

$$K_1(t, t_0) = \frac{a\pi}{2C}[G_1(a(t - t_0)) - iG_2(a(t - t_0))],$$
$$K_2(t, t_0) = \frac{a\pi}{2C}[G_1(a(t - t_0)) + iG_2(a(t - t_0))],$$
$$K_3(t, t_0) = \frac{h_2}{2}\left[E\left(at, \frac{h_2(t_0 - 1)}{2}\right) + \frac{\pi}{C}G_3\left(at; \frac{h_2(t_0 - 1)}{2}\right)\right],$$
$$K_4(t, t_0) = \frac{h_2}{2}\left[F\left(\frac{h_2(t-1)}{2}, \frac{h_2(t_0 - 1)}{2}\right) - \frac{\pi(1 + \alpha)}{C(1 - \beta^2)} \times H_3\left(\frac{h_2(t-1)}{2}; \frac{h_2(t_0 - 1)}{2}, 0\right)\right],$$

$$K_5(t, t_0) = -\frac{a(1+\alpha)}{2(1-\beta^2)}\left\{D(y, -x_0) + \frac{\pi}{C}[H_1(y; -x_0) - iH_2(y; -x_0)]\right\},$$

$$K_6(t, t_0) = \overline{K_5(t, t_0)},$$

$$p_1(t) = -\pi Q(at),$$

$$p_2(t) = \frac{1+\alpha}{1-\beta^2}\pi R\left(\frac{h_2(t-1)}{2}\right). \tag{28}$$

If the vertical crack is not present, B_2 is set equal to zero and only the first equation of (26) is enforced. If the interface crack is not present, on the other hand, the first of Eqns. (26) is not enforced and B_1 is set equal to zero in the second equation. For the edge crack whose length $c < h_2$, the dislocation density is instead represented as $B_2(t) = B_{2x}(c(t-1)/2)$, and in the expression of the kernel K_4 given by (28) h_2 needs to be replaced by c. Other loading conditions can be treated by modifying functions p_1 and p_2.

The integral equations can be solved numerically by representing each dislocation density in terms of a regular function and a characteristic function with the proper singularities at the end points. Thus, let

$$B_1(t) = \frac{\phi_1(t)}{(1-t)^{\gamma}(1+t)^{1-\gamma}}, \quad B_2(t) = \frac{\phi_2(t)}{(1-t)^{\lambda}\sqrt{1+t}}, \tag{29}$$

where $\phi_1(t)$ and $\phi_2(t)$ are regular continuous functions which are approximated as piecewise quadratic [13], and

$$\gamma = \frac{1}{2} + i\varepsilon, \qquad \varepsilon = \frac{1}{2\pi}\log\frac{1-\beta}{1+\beta}. \tag{30}$$

The exponent λ is taken as 0.5 for the T-crack (Fig. 1a) and for an edge crack whose tip does not touch the interface (Fig. 1c, d). If the tip of the edge crack touches the interface, λ is determined by the following characteristic equation [14, 15]:

$$\cos\pi\lambda - \frac{2(\beta-\alpha)}{1+\beta}(1-\lambda)^2 - \frac{\alpha+\beta^2}{1-\beta^2} = 0. \tag{31}$$

Using the method developed by Miller and Keer [13], integral equations (26) can be reduced to a set of algebraic equations.

The additonal conditions to be satisfied are as follows. For the T-crack

$$\int_{-1}^{1} B_{1y}(t)\,\mathrm{d}t = 0, \tag{32}$$

$$\phi_2(\pm 1) = 0, \tag{33}$$

$$\int_{-1}^{1} B_{1x}(t)\,\mathrm{d}t \neq 0. \tag{34}$$

Equation (32) is the closure condition for the horizontal crack, (33) represents the condition that the stress singularities at the tips of the vertical notch are less than square root, and (34) implies the bluntness at $x = 0$. As will be discussed in the next section, the representation of the dislocation density for the T-crack is not rigorous. However, the error introduced is acceptable for the configurations considered in this paper.

For a single interface crack

$$\int_{-1}^{1} B_1(t)\,\mathrm{d}t = 0 \tag{35}$$

and for a single edge crack

$$\phi_2(-1) = 0, \tag{36}$$

$$\int_{-1}^{1} B_{2x}(t)\,\mathrm{d}t \neq 0. \tag{37}$$

4. Numerical results and stress intensity factor analysis

The stress intensity factor K of the interface crack (Fig. 1b) and the T-crack (Fig. 1a) are defined by [16]

$$K = \lim_{x \to a} \{\sqrt{2\pi(x-a)}(x-a)^{-i\varepsilon}[\sigma_{yy}(x,0) + i\sigma_{xy}(x,0)]\}. \tag{38}$$

It can be shown that in terms of $\phi_1(t)$, which is determined by (26) with (28) and (29), this complex stress intensity factor can be expressed as

$$K = \frac{ip}{h_2}\sqrt{\pi a(1-\beta^2)}(2a)^{-i\varepsilon}\overline{\phi_1(1)}, \tag{39}$$

for the four point bending load. For an edge crack whose tip does not touch the interface

$$K = \lim_{y \to (c-h_2)} [\sqrt{2\pi(h_2 + y - c)}\sigma_{xx}(0, y)] \tag{40}$$

and similarly in terms of $\phi_2(t)$

$$K = \frac{p}{h_2}\frac{(1-\beta^2)}{(1+\alpha)}\sqrt{\pi c/2}\phi_2(1), \tag{41}$$

for the four point bending. For an edge crack whose tip touches the interface

$$K = \lim_{y \to 0} [\sqrt{2\pi}y^{\lambda}\sigma_{xx}(0, y)] \tag{42}$$

and

$$K = \frac{p}{h_2}\frac{(1-\beta^2)}{(1+\alpha)}\sqrt{\pi}(h_2/2)^{\lambda}\phi_2(1). \tag{43}$$

For the other loading cases, the factor p/h_2 in (39), (41) and (43) is replaced correspondingly.

The energy release rate of the interface cracks in the considered plane strain problems is given by [17]

$$G = [(1-\nu_1)/\mu_1 + (1-\nu_2)/\mu_2]K\bar{K}/4\cosh^2(\pi\varepsilon). \tag{44}$$

In order to check the lengthy algebra and the numerical scheme, two configurations which have previously been analyzed are considered first: a pressurized crack between two bonded dissimilar layers and a pressurized vertical edge crack in the bottom layer of a composite beam. Figure 2 shows the dimensionless stress intensity factors $\hat{K}/\sigma_0\sqrt{a} = \lim_{x\to a}[(a-x)^{1-\gamma}(a+x)^{\gamma}(\sigma_{yy}+i\sigma_{xy})]/\sigma_0 a$ versus $0.1 \leqslant h_1/2a \leqslant 4$ for the interface crack with $h_2/h_1 = 3$, $\nu_1 = \nu_2 = 0.3$, $\mu_1/\mu_2 = 3$ and $\mu_1/\mu_2 = 10$, respectively. The results are plotted in terms of this definition of stress intensity factor for comparison with [18]. For $h_1/2a > 0.5$ the results agree with those presented in [18] (no results were given there for $h_1/2a < 0.5$). As expected, when the crack becomes shorter, the stress intensity factor converges to $1 + 2i\varepsilon$ which is the solution for an interface crack between two bonded half-spaces.

For the edge crack problem a homogeneous beam and four ceramic composite strips are considered. They are: strip 1 Ti/Al_2O_3 with $\nu_1 = 0.322$, $\nu_2 = 0.207$ and $\mu_2/\mu_1 = 4.129$, strip 2 Ni/MgO with $\nu_1 = 0.314$, $\nu_2 = 0.175$ and $\mu_2/\mu_1 = 1.588$, strip 3 MgO/Ni and strip

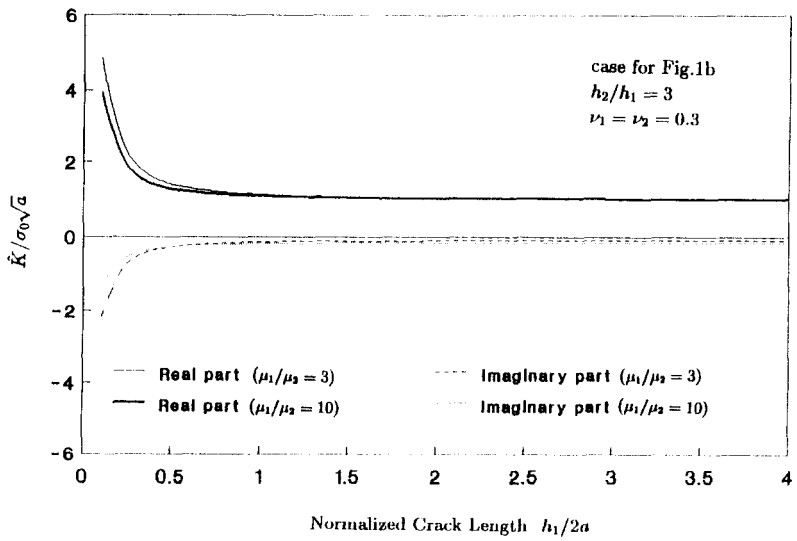

Fig. 2. Stress intensity factors for an interface crack under uniform pressure.

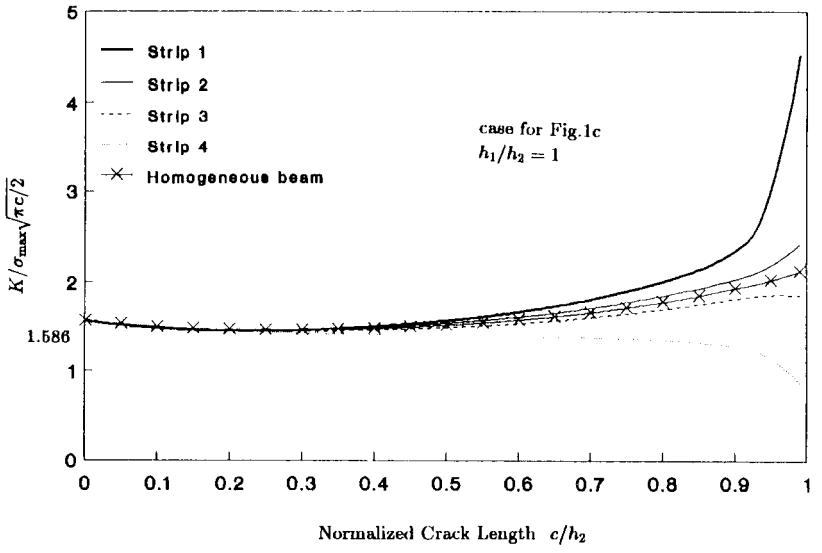

Fig. 3. Stress intensity factors for an edge crack under four point bending.

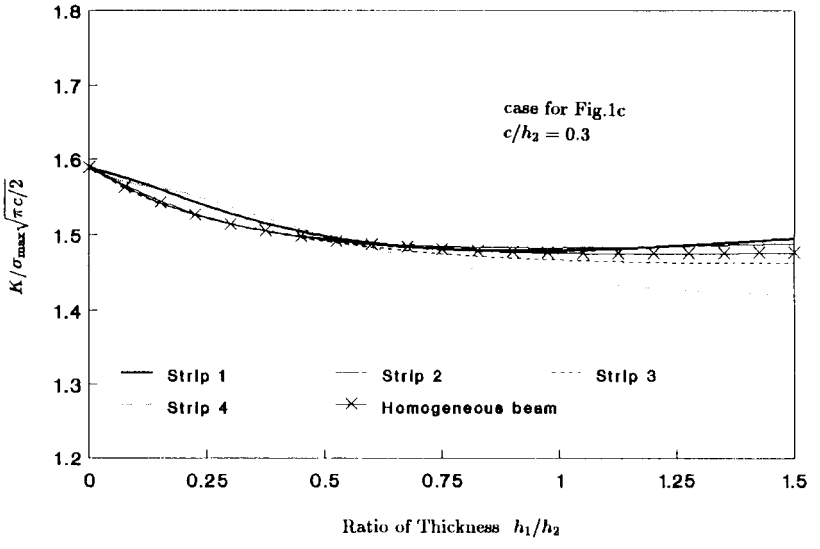

Fig. 4. Effect of relative thickness of the strips on the stress intensity factors of an edge crack under four point bending.

4 Al_2O_3/Ti [16]. Figures 3 and 4 show the dimensionless stress intensity factors as functions of crack length and relative thickness of the layers for the four point bending case considered in [3, 4] where $d = 5h_2$, $e = 8\frac{1}{3}h_2$ and $l = 3\frac{1}{3}h_2$. The quantity σ_{max} is the axial stress at the lower surface of the composite beam calculated using composite beam theory. It is given by

$$\sigma_{max} = \frac{MmH_2}{(I_1 + mI_2)}, \tag{45}$$

with

$$m = \frac{\mu_2(1-\nu_1)}{\mu_1(1-\nu_2)}, \quad \delta = h_1/h_2,$$

$$H_1 = h_1 + h_2 - H_2, \quad H_2 = \frac{h_2}{2(m+\delta)}(m + 2\delta + \delta^2),$$

$$I_1 = \frac{1}{12}h_1^3 + h_1\left(H_1 - \frac{h_1}{2}\right)^2, \quad I_2 = \frac{1}{12}h_2^3 + h_2\left(H_2 - \frac{h_2}{2}\right)^2. \tag{46}$$

where M is the bending moment; for the four point bending shown in Fig. 1 $M = pl/2$. It is observed that as the crack tip approaches the interface, the stress intensity factor increases drastically if the edge crack is in the stiffer layer. In the limit, the stress intensity factor approaches infinity for this case, since it can be shown that as the crack tip hits the interface the stress singularity is greater than square root. When the crack is in the softer layer, the stress intensity factor goes to zero as the tip approaches the interface, since the singularity in this case is less than square root. When the crack is very short, namely $c/h_2 \to 0$, the dimensionless stress intensity factor approaches 1.586, which corresponds to the solution of an edge crack in a half-space under uniform tension. When the thickness of the upper layer becomes very thin, the stress intensity factors for the bimaterial strips approach those for a homogeneous beam. It is interesting to note that for these values of mismatch, the dimensionless stress intensity factors are insensitive to c/h_2 for $c/h_2 < 0.5$ and insensitive to h_1/h_2 for $h_1/h_2 > 1$. Results were also obtained for three point bending. For this geometry the nondimensional results were found to be almost exactly the same as for the four point bending.

Figure 5 shows the stress intensity factors for the edge crack whose tip touches the interface. In this case the singularity depends on the elastic mismatch of the two layers and factor λ is

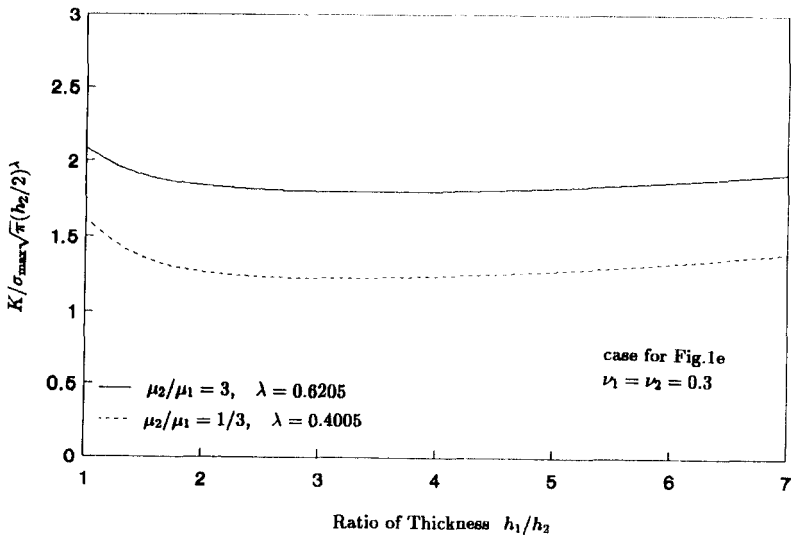

Fig. 5. Effect of relative thickness on the stress intensity factors of an edge crack whose tip touches the interface (four point bending).

calculated from (31). For the combination considered here $\nu_1 = \nu_2 = 0.3$, $\mu_2/\mu_1 = 3$ and $\mu_2/\mu_1 = \frac{1}{3}$, and singularities $\lambda = 0.6205$ and $\lambda = 0.4005$, respectively. Notice that, since the stress singularities are different, it is meaningless to directly compare the values of the dimensionless stress intensity factors given in Figs. 4 and 5. It should be noted that these results do not compare at all with those in [5, 6].

Suppose that a bimaterial beam is subjected to a concentrated force p along its neutral axis as shown in Fig. 1f where H_1 and H_2 are given by (46). The longitudial stress across the lower layer is

$$\sigma^{(2)} = \frac{p}{h_2(1 + \delta\Sigma)}, \tag{47}$$

where $\Sigma = \mu_1(1 - \nu_2)/[\mu_2(1 - \nu_1)]$. If the beam is subjected to the remote bending, based on the composite beam theory, the stress on the lower layer is

$$\sigma_x = \sigma_{\max}\frac{H_2 - h_2 - y}{H_2}, \tag{48}$$

Table 1. Stress intensity factors for edge crack under tension along neutral axis ($c/h_2 = 0.5$)

		$K/\sigma^{(2)}\sqrt{\pi c/2}$								
		α								
h_1/h_2	β	−0.8	−0.6	−0.4	−0.2	0.0	0.2	0.4	0.6	0.8
	−0.4	3.891	3.786							
	−0.3	3.892	3.788	3.681	3.571					
	−0.2	3.893	3.791	3.685	3.576	3.463	3.345			
	−0.1	3.894	3.793	3.688	3.581	3.469	3.353	3.231	3.102	
0.1	0.0	3.895	3.795	3.692	3.585	3.474	3.360	3.240	3.112	2.967
	0.1			3.695	3.589	3.480	3.366	3.248	3.122	2.979
	0.2					3.485	3.373	3.255	3.131	2.991
	0.3							3.262	3.139	3.001
	0.4									3.011
	−0.4	2.782	2.435							
	−0.3	2.828	2.481	2.284	2.146					
	−0.2	2.866	2.520	2.322	2.181	2.066	1.964			
	−0.1	2.900	2.554	2.354	2.211	2.094	1.989	1.886	1.773	
1	0.0	2.929	2.584	2.383	2.237	2.117	2.010	1.903	1.786	1.635
	0.1			2.408	2.260	2.138	2.027	1.917	1.794	1.637
	0.2					2.155	2.041	1.927	1.800	1.636
	0.3							1.933	1.801	1.629
	0.4									1.618
	−0.4	2.117	1.894							
	−0.3	2.137	1.910	1.774	1.678					
	−0.2	2.149	1.920	1.783	1.685	1.610	1.549			
	−0.1	2.157	1.924	1.786	1.687	1.611	1.549	1.498	1.453	
10	0.0	2.158	1.924	1.784	1.684	1.608	1.545	1.493	1.449	1.410
	0.1			1.778	1.677	1.600	1.537	1.485	1.440	1.401
	0.2					1.588	1.525	1.472	1.427	1.388
	0.3							1.454	1.409	1.370
	0.4									1.346

where σ_{max} and H_2 are given in (45) and (46). Notice that two Dundurs parameters α and β can cover the elastic moduli dependence of a two-dimensional bimaterial system [19]. In Table 1 and Table 2 the stress intensity factors are given in terms of α and β for an edge crack with $c/h_2 = 0.5$ under the above two loading systems. Table 3 shows the singularity λ of the edge

Table 2. Stress intensity factors for edge crack under pure bending ($c/h_2 = 0.5$)

		$K/\sigma_{max}\sqrt{\pi c/2}$								
		α								
h_1/h_2	β	−0.8	−0.6	−0.4	−0.2	0.0	0.2	0.4	0.6	0.8
	−0.4	2.074	2.032							
	−0.3	2.074	2.034	1.996	1.960					
	−0.2	2.075	2.036	1.998	1.964	1.934	1.913			
	−0.1	2.076	2.037	2.000	1.967	1.938	1.918	1.910	1.924	
0.1	0.0	2.077	2.038	2.002	1.969	1.942	1.922	1.916	1.931	1.982
	0.1			2.004	1.972	1.945	1.927	1.921	1.938	1.991
	0.2					1.949	1.931	1.926	1.944	1.999
	0.3							1.931	1.950	2.008
	0.4									2.015
	−0.4	1.594	1.509							
	−0.3	1.625	1.543	1.510	1.487					
	−0.2	1.652	1.572	1.539	1.514	1.488	1.457			
	−0.1	1.675	1.597	1.564	1.538	1.511	1.477	1.434	1.373	
1	0.0	1.695	1.619	1.585	1.559	1.530	1.495	1.448	1.383	1.283
	0.1			1.605	1.577	1.547	1.509	1.460	1.391	1.285
	0.2					1.561	1.521	1.468	1.396	1.284
	0.3							1.474	1.397	1.278
	0.4									1.269
	−0.4	1.945	1.771							
	−0.3	1.963	1.786	1.669	1.583					
	−0.2	1.975	1.796	1.677	1.590	1.521	1.464			
	−0.1	1.982	1.800	1.680	1.592	1.522	1.465	1.417	1.375	
10	0.0	1.984	1.800	1.679	1.589	1.519	1.461	1.413	1.371	1.334
	0.1			1.673	1.582	1.512	1.454	1.405	1.363	1.326
	0.2					1.500	1.441	1.392	1.350	1.313
	0.3							1.375	1.333	1.296
	0.4									1.273

Table 3. Singularity for edge crack whose tip touches the interface

	λ								
	α								
β	−0.8	−0.6	−0.4	−0.2	0.0	0.2	0.4	0.6	0.8
−0.4	0.7321	0.6449							
−0.3	0.7394	0.6507	0.5949	0.5567					
−0.2	0.7438	0.6533	0.5946	0.5533	0.5230	0.5000			
−0.1	0.7456	0.6529	0.5912	0.5467	0.5135	0.4881	0.4682	0.4523	
0.0	0.7450	0.6495	0.5843	0.5364	0.5000	0.4718	0.4496	0.4318	0.4173
0.1			0.5734	0.5213	0.4812	0.4498	0.4249	0.4049	0.3887
0.2					0.4551	0.4196	0.3913	0.3687	0.3504
0.3							0.3435	0.3173	0.2963
0.4									0.2114

Table 4. Stress intensity factors for edge crack whose tip touches the interface (tension along neutral axis)

		$K/\sigma^{(2)}\sqrt{\pi}(h_2/2)^{\lambda}$								
		α								
h_1/h_2	β	−0.8	−0.6	−0.4	−0.2	0.0	0.2	0.4	0.6	0.8
	−0.4	42.29	64.73							
	−0.3	36.34	57.24	65.37	66.57					
	−0.2	31.86	51.88	59.99	61.77	59.26	53.75			
	−0.1	28.41	48.00	56.27	58.63	56.83	52.00	44.82	35.58	
0.1	0.0	25.70	45.26	53.86	56.87	55.76	51.48	44.67	35.59	23.71
	0.1			52.70	56.49	56.14	52.38	45.77	36.57	24.27
	0.2					58.45	55.26	48.70	39.02	25.72
	0.3							55.06	44.28	28.90
	0.4									36.76
	−0.4	6.209	6.483							
	−0.3	5.631	5.901	5.625	5.120					
	−0.2	5.182	5.442	5.238	4.819	4.300	3.741			
	−0.1	4.820	5.074	4.927	4.579	4.123	3.613	3.078	2.524	
1	0.0	4.523	4.775	4.679	4.393	3.993	3.526	3.020	2.487	1.918
	0.1			4.488	4.262	3.914	3.485	3.004	2.484	1.921
	0.2					3.904	3.512	3.049	2.532	1.963
	0.3							3.210	2.681	2.082
	0.4									2.417
	−0.4	2.465	2.351							
	−0.3	2.286	2.189	2.064	1.931					
	−0.2	2.149	2.063	1.962	1.851	1.738	1.629			
	−0.1	2.042	1.965	1.883	1.791	1.693	1.595	1.500	1.413	
10	0.0	1.958	1.890	1.825	1.750	1.666	1.577	1.489	1.405	1.326
	0.1			1.790	1.732	1.662	1.582	1.499	1.416	1.336
	0.2					1.689	1.621	1.542	1.458	1.375
	0.3							1.649	1.563	1.471
	0.4									1.726

crack whose tip touches the interface. The corresponding stress intensity factors are given for this class of edge cracks.

Figures 6 snd 7 show the stress intensity factors of the edge cracks for the thermal loading case. The sign of the stress intensity factor changes when the crack length is approximately equal to $0.6h_2$ as a result of bending. If additional loads are superimposed, these results suggest that crack growth can either be accelerated when $(\alpha_2 - \alpha_1)\Delta T < 0$ or slowed down when $(\alpha_2 - \alpha_1)\Delta T > 0$ by the introduction of a temperature change.

The last example considers the T-crack, which is referred to as the Santa Barbara specimen, shown in Fig. 1a where $d = 5h_2$, $e = 8\frac{1}{3}h_2$ and $l = 3\frac{1}{3}h_2$. Results were calculated for crack lengths which are shorter than those presented in [3, 4]. Figures 8–14 show the dimensionless stress intensity factors $Kh^{i\varepsilon}h^{3/2}/pl$, energy release rates G and the phase angles, defined as the argument of $Kh^{i\varepsilon}$, for strips with $\nu_1 = \nu_2 = 0.3$ and $\mu_1/\mu_2 = 1$, $\mu_1/\mu_2 = 2.5$, $\mu_1/\mu_2 = 5$, $\mu_1/\mu_2 = 10$, respectively. The results obtained in [3, 4] for $a/h_2 > 0.5$ are superposed on the figures. The agreement is observed to be quite good. It is observed that steady state begins at crack lengths equal to h_2. Results for a/h_2 less than 0.1 were not calculated because we believe that accurate solutions cannot be obtained for these cases using the present formulation, since the integral equations are coupled. To obtain accurate results for small value of a/h_2 one would need to formulate the problem in terms

Table 5. Stress intensity factors for edge crack whose tip touches the interface (pure bending)

		$K/\sigma_{max}\sqrt{\pi}(h_2/2)^{\lambda}$								
		α								
h_1/h_2	β	−0.8	−0.6	−0.4	−0.2	0.0	0.2	0.4	0.6	0.8
	−0.4	12.59	20.29							
	−0.3	10.71	17.87	21.27	22.67					
	−0.2	9.280	16.13	19.47	20.99	21.25	20.56			
	−0.1	8.165	14.86	18.20	19.87	20.33	19.85	18.56	16.35	
0.1	0.0	7.279	13.94	17.36	19.22	19.90	19.61	18.46	16.33	12.51
	0.1			16.93	19.03	19.98	19.90	18.87	16.74	12.77
	0.2					20.73	20.94	20.02	17.81	13.50
	0.3							22.56	20.14	15.10
	0.4									19.11
	−0.4	1.739	2.478							
	−0.3	1.538	2.215	2.536	2.605					
	−0.2	1.379	2.004	2.324	2.417	2.353	2.182			
	−0.1	1.247	1.830	2.147	2.260	2.223	2.077	1.855	1.572	
1	0.0	1.134	1.683	1.999	2.130	2.116	1.994	1.790	1.552	1.188
	0.1			1.874	2.024	2.033	1.932	1.745	1.487	1.160
	0.2					1.979	1.900	1.727	1.475	1.148
	0.3							1.758	1.505	1.166
	0.4									1.266
	−0.4	2.095	2.077							
	−0.3	1.937	1.927	1.841	1.734					
	−0.2	1.815	1.810	1.744	1.656	1.561	1.468			
	−0.1	1.719	1.718	1.668	1.596	1.515	1.431	1.350	1.274	
10	0.0	1.643	1.647	1.611	1.554	1.485	1.409	1.334	1.260	1.191
	0.1			1.573	1.531	1.474	1.406	1.335	1.263	1.194
	0.2					1.489	1.432	1.364	1.292	1.220
	0.3							1.447	1.372	1.293
	0.4									1.497

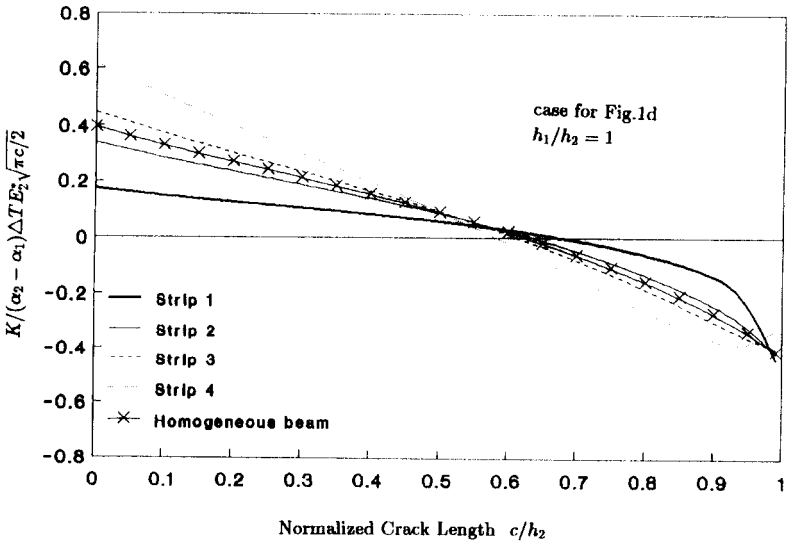

Fig. 6. Stress intensity factors for an edge crack under thermal stresses.

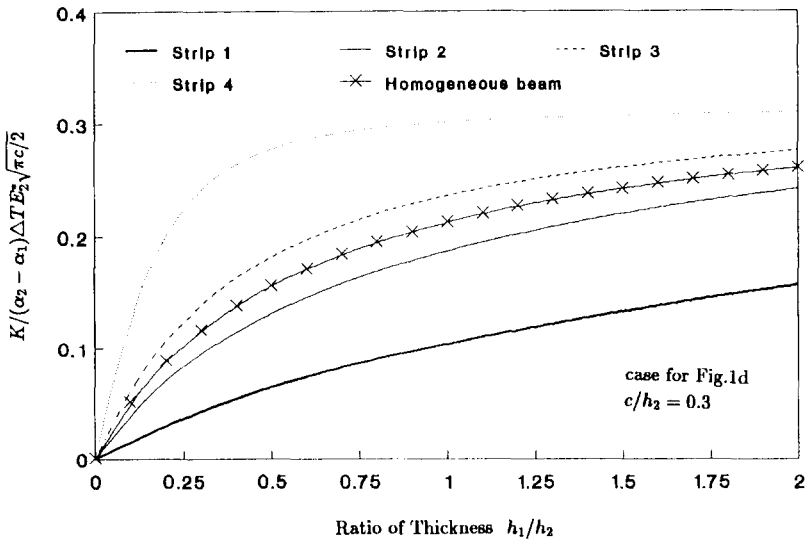

Fig. 7. Effect of relative thickness of the strips on the stress intensity factors of an edge crack under four point bending.

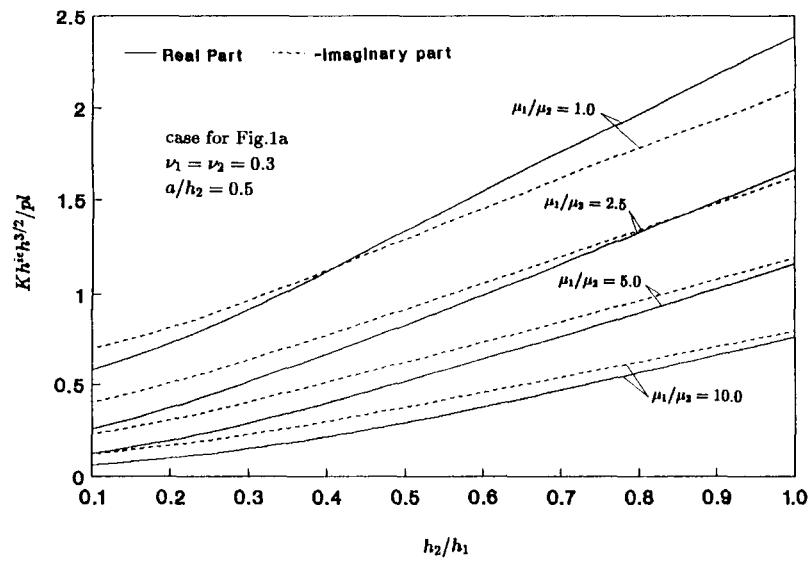

Fig. 8. Stress intensity factors for a T-crack under four point bending ($\mu_1/\mu_2 = 1$).

of a single integral equation whose kernel includes an analytic solution for the interaction of the two cracks.

It should be mentioned that for crack lengths greater than $1.5h_2$ convergent results were not obtained as a result of using a distribution of dislocations density which is continuous at $x = 0$, $y = 0$. Because the vertical crack intersects the interface crack, the slope of the horizontal crack is discontinuous at $(0, 0)$. The numerical scheme implicitly assumes that the slope there is zero. We believe it is this error which leads to poor results for long crack lengths, for which the slope at $(0, 0)$ is definitely not zero. This problem is being ad-

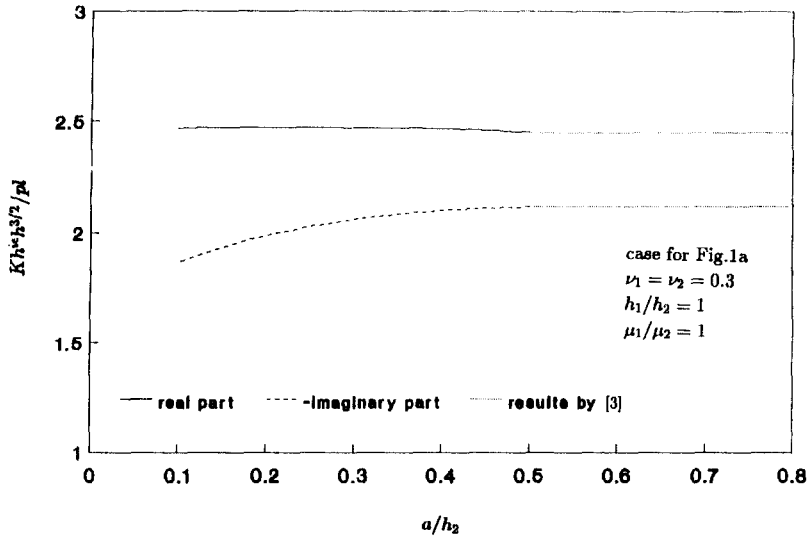

Fig. 9. Stress intensity factors for a T-crack under four point bending ($\mu_1/\mu_2 = 2.5$).

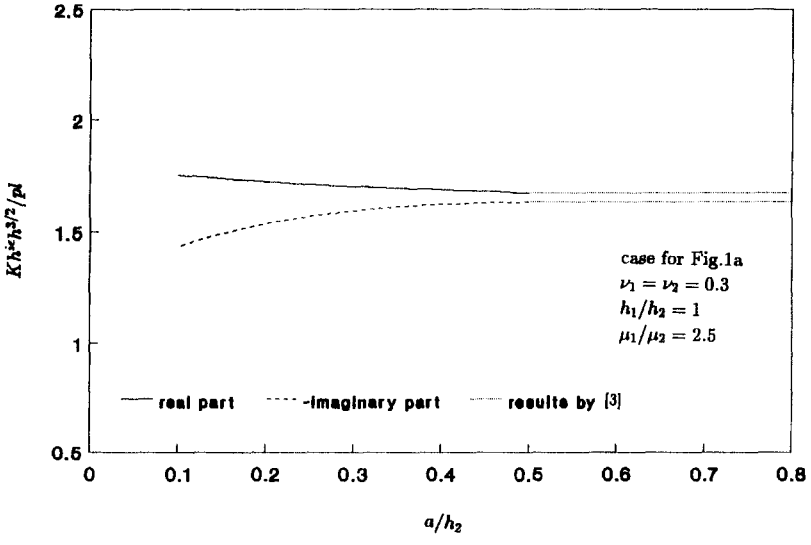

Fig. 10. Stress intensity factors for a T-crack under four point bending ($\mu_1/\mu_2 = 5$).

dressed by the authors at the present time by introducing a discontinuous distribution of dislocations.

5. Conclusions

An analytical formulation has been presented which can be used to solve a class of plane elastostatic problems involving cracked bimaterial beams. Results were calculated only for a few

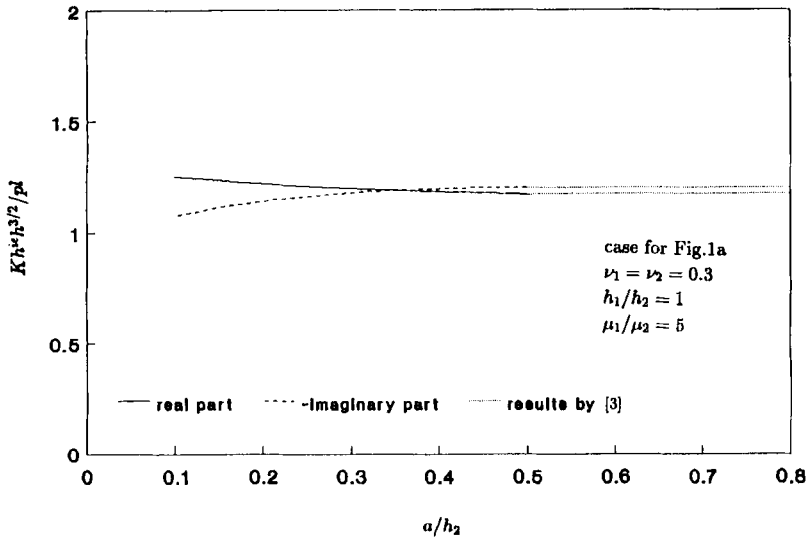

Fig. 11. Stress intensity factors for a T-crack under four point bending ($\mu_1/\mu_2 = 10$).

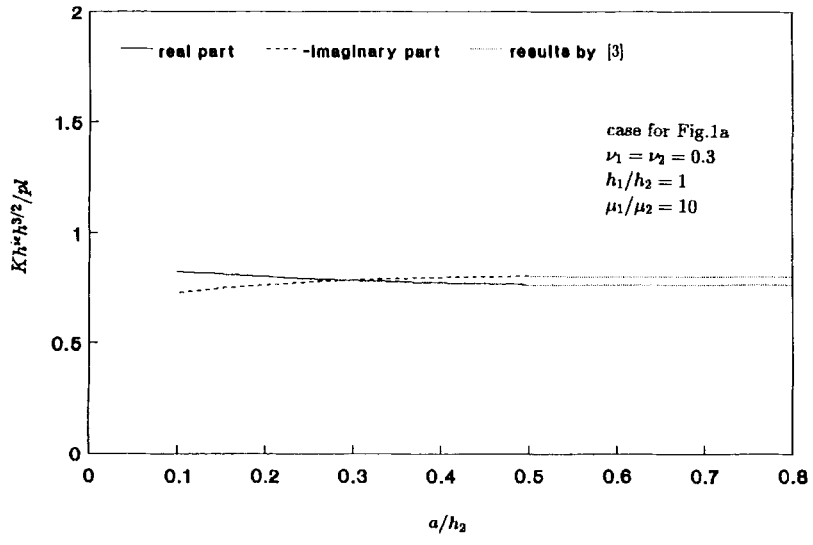

Fig. 12. Effect of relative thickness of the strips on the stress intensity factors of a T-crack under four point bending.

geometric configurations and symmetric loadings. However, since the analysis relies on fundamental solutions for dislocations on bonded strips, other configurations such as inclined or curved cracks and/or non-symmetric loadings can be treated with minor modifications. For the T-crack, when the interface crack is relatively short, the results obtained using the singular integral equation approach compare very well with those obtained in [3, 4] using the finite element method. However, for such configurations, which involve discontinuous dislocation densities at the intersection of the two cracks, poor results were obtained for relatively long

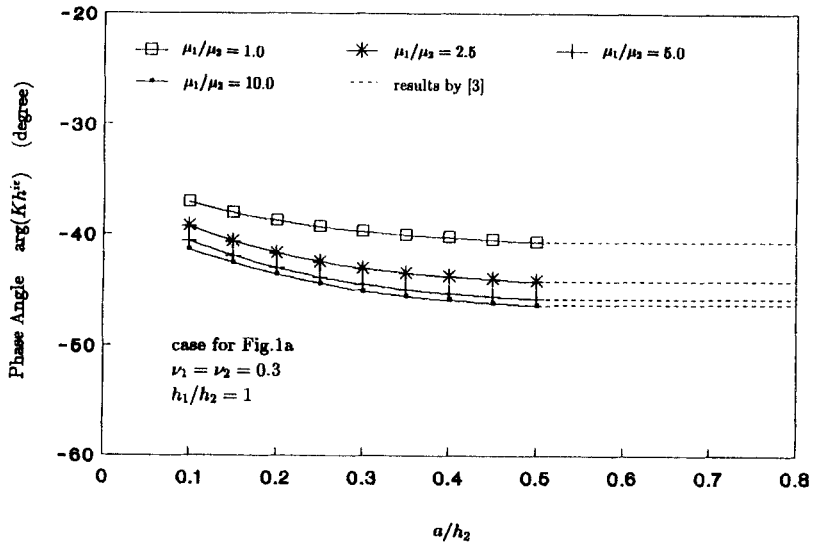

Fig. 13. Energy release rates of a T-crack under four point bending.

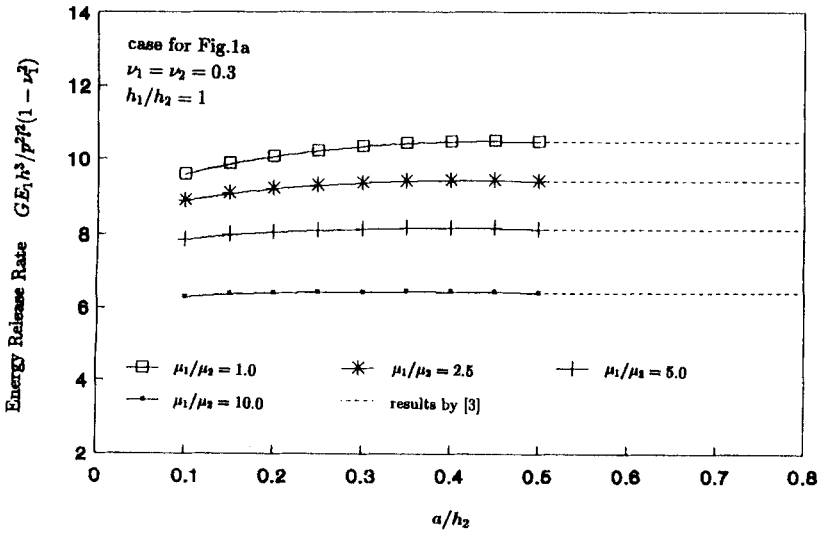

Fig. 14. Phase angles of a T-crack under four point bending.

interface cracks. This problem can be treated by modifying the numerical scheme to handle discontinuous dislocation densities.

Appendix

For dislocation b_x lying at interface (0, 0)

$$f_1(\xi) = \frac{Cb_x}{4\mu_1}[\beta + (1+\beta)h_1\xi]e^{-h_1\xi},$$

$$f_2(\xi) = -\frac{Cb_x}{4\mu_1}[1-(1+\beta)h_1\xi]\mathrm{e}^{-h_1\xi},$$

$$f_3(\xi) = -\frac{Cb_x}{4\mu_2}[\beta-(1-\beta)h_2\xi]\mathrm{e}^{-h_2\xi},$$

$$f_4(\xi) = -\frac{Cb_x}{4\mu_2}[1-(1-\beta)h_2\xi]\mathrm{e}^{-h_2\xi}. \tag{A.1}$$

For dislocation b_y lying at interface $(0, 0)$

$$f_1(\xi) = \frac{Cb_y}{4\mu_1}[1+(1+\beta)h_1\xi]\mathrm{e}^{-h_1\xi},$$

$$f_2(\xi) = -\frac{Cb_y}{4\mu_1}[\beta-(1+\beta)h_1\xi]\mathrm{e}^{-h_1\xi},$$

$$f_3(\xi) = \frac{Cb_y}{4\mu_2}[1+(1-\beta)h_2\xi]\mathrm{e}^{-h_2\xi},$$

$$f_4(\xi) = -\frac{Cb_y}{4\mu_2}[\beta+(1-\beta)h_2\xi]\mathrm{e}^{-h_2\xi}. \tag{A.2}$$

For dislocation b_x lying at $(0, \zeta)$ with $\zeta < 0$

$$f_1(\xi) = \frac{Cb_x}{4\mu_1}[\beta+(h_1-\zeta)\xi+(h_1+\zeta)\beta\xi]e^{-(h_1-\zeta)\xi}$$

$$f_2(\xi) = -\frac{Cb_x}{4\mu_1}[1-(1+\beta)(h_1-\zeta)\xi-2\beta\zeta\xi]e^{-(h_1-\zeta)\xi}$$

$$\begin{aligned} f_3(\xi) = &-\frac{Cb_x}{4\mu_2(1+\alpha)}[(1-\beta^2)(h_2+\zeta)\xi e^{-(h_2+\zeta)\xi} \\ &+\frac{Cb_x}{4\mu_2(1+\alpha)}[\beta(1+\alpha)-(\alpha-\beta)(1-\beta)(h_2+\zeta)\xi \\ &-2(\alpha-\beta)(1-\beta)h_2\zeta\xi^2]e^{-(h_2-\zeta)\xi} \end{aligned}$$

$$\begin{aligned} f_4(\xi) = &-\frac{Cb_x(1-\beta^2)}{4\mu_2(1+\alpha)}[1-(h_2+\zeta)\xi]e^{-(h_2+\zeta)\xi} \\ &-\frac{Cb_x}{4\mu_2(1+\alpha)}[(\alpha+\beta^2)-(\alpha-\beta)(1-\beta)(h_2-\zeta)\xi \\ &-2(\alpha-\beta)(1-\beta)\zeta h_2\xi^2]e^{-(h_2-\zeta)\xi}. \end{aligned} \tag{A.3}$$

For four-point bending

$$f_1(\xi) = -\frac{p}{4\mu_1}\cos\xi d, \qquad f_2(\xi) = 0$$

$$f_3(\xi) = -\frac{p}{4\mu_2}\cos\xi e, \qquad f_4(\xi) = 0. \tag{A.4}$$

Acknowledgement

Financial support was provided by the Defence Advanced Research Projects Agency through the University Research Initiative Program of C.W.R.U. under ONR Contract N-0013-86-K-0773 and by Lewis Research Center under Grant NAG3-856. The computations were performed on a Cray which was made available through a grant from the Ohio Supercomputer Center.

References

1. A.G. Evans and D.B. Marshall, *Acta Metallurgica* 37 (1989) 2567–2583.
2. M.-Y. He and J.W. Hutchinson, *International Journal of Solids and Structures* 25 (1989) 1053–1067.
3. P.G. Charalambides, J. Lund, A.G. Evans and R.M. McMeeking, ASME *Journal of Applied Mechanics* 56 (1989) 77–82.
4. P.P.L. Matos, R.M. McMeeking, P.G. Charalambides and M.D. Drory, *International Journal of Fracture* 40 (1989) 235–254.
5. M.-C. Lu, Ph.D. dissertation, Lehigh University (1978).
6. M.-C. Lu and F. Erdogan, *Engineering Fracture Mechanics* 18 (1983) Part I, 491–506; Part II, 507–528.
7. R. Ballarini, D.J. Mukai and G.R. Miller, NASA Contractor Report 182273 (1989), also *ASME Journal of Applied Mechanics* 57 (1990) 887–893.
8. M. Comninou, *Philosophical Magazine* 36 (1977) 1281–1283.
9. I.N. Sneddon, *Fourier Transforms*, McGraw Hill, New York (1951).
10. R. Ballarini, S.P. Shah and L.M. Keer, *Engineering Fracture Mechanics* 20 (1984) 433–445.
11. P.D. Copp, Ph.D. dissertation, Northwestern University (1986).
12. B.A. Boley and J.H. Weiner, *Theory of Thermal Stresses*, John Wiley & Sons (1960).
13. G.R. Miller and L.M. Keer, *Quarterly of Applied Mathematics* 42 (1985) 455–465.
14. T.S. Cook and F. Erdogan, *International Journal of Engineering Science* 10 (1972) 677–697.
15. F. Erdogan and V. Biricikoglu, *International Journal of Engineering Science* 10 (1973) 745–766.
16. J.W. Hutchinson, M. Mear and J.R. Rice, ASME *Journal of Applied Mechanics* 54 (1988) 828–832.
17. B.M. Malyshev and R.L. Salganik, *International Journal of Fracture Mechanics* 1 (1965) 114–128.
18. F. Erdogan and G.D. Gupta, *International Journal of Solids & Structures* 7 (1971) 1089–1107.
19. J. Dundurs, in *Mathematical Theory of Dislocations*, American Society of Mechanical Engineering, New York (1969) 70–115.